Applied Physics Letters ARTICLE pubs.aip.org/aip/apl

Dual-polarized angle-selective surface based on double-layer frequency selective surface

Cite as: Appl. Phys. Lett. **124**, 111701 (2024); doi: 10.1063/5.0176430
Submitted: 13 September 2023 · Accepted: 24 February 2024 ·
Published Online: 11 March 2024

Chao Du,[1,2] Huizhen Chen,[3] Shaofei Wang,[4] Yongqiang Pang,[1] Tao Zhou,[5] Song Xia,[1] and Di Zhou[1,a)]

AFFILIATIONS

[1]Multifunctional Materials and Structures, Key Laboratory of the Ministry of Education, School of Electronic Science and Engineering, Xi'an Jiaotong University, Xi'an, Shaanxi 710049, China
[2]School of Electrical and Electronic Engineering, Nanyang Technological University, Singapore 639798
[3]School of Information Engineering, Shaanxi Institute of International Trade & Commerce, Xi'an, Shaanxi 712046, China
[4]School of Information and Communications Engineering, Xi'an Jiaotong University, Xi'an, Shaanxi 710049, China
[5]School of Electronic and Information Engineering, Hangzhou Dianzi University, Hangzhou 310018, China

[a)]Author to whom correspondence should be addressed: zhoudi1220@gmail.com

ABSTRACT

In this Letter, we propose a dual-polarized angle-selective surface (ASS) based on a double-layer frequency selective surface (FSS) to achieve angular selectivity. By appropriately constructing the structure of the single-layer FSS, bandpass and band-stop are produced by the ASS under normal and oblique incidences, respectively, resulting in exceptional angular selectivity. Simulated results show that the proposed low-pass ASS achieves a bandpass ($|S_{21}| > -1$ dB) from 0° to 10° and a band-stop ($|S_{21}| < -20$ dB) from 31° to 85° with a profile thickness of 0.6 λ. A low-pass ASS prototype with an operating frequency of 10 GHz is fabricated to demonstrate the design concept. The measured results of the transmission coefficients are in good agreement with the simulated results. The proposed ASS can play an important role in many applications, as in minimizing the side lobes of the antenna.

The ability to manipulate electromagnetic (EM) waves has long been a major scientific and technological goal.[1–3] Over the last few decades, manipulation of electromagnetic waves focuses on the three fundamental properties of frequency,[4,5] polarization,[6,7] and propagation direction.[8,9] According to these separate properties, tremendous progress has been made in both polarization selectivity and frequency selectivity. The angular selectivity that allows electromagnetic waves under certain incidence angles to transmit while reflecting waves under other incident angles has been developed in many optical systems.[10,11] However, when the operating frequency is downshifted from the optical to microwave regime, the profile of angular selectivity structure will be extremely bulky.[12–15]

Based on the angular selectivity, researchers have proposed a number of ways to achieve the property. The use of geometrical optics is a traditional method of achieving angular selectivity. For example, by limiting the emission angle of a high-quality GaAs solar cell, Kosten *et al.*[3] achieved power conversion efficiencies above 38% with a single junction. In addition, Atwater *et al.*[16] proposed a reflective broadband angle-selective filter consisting of parabolic directors, which achieves the performance that incident light is funneled at incidence angles less than 5.6° and strongly reflected at larger incidence angles. However, the performance of systems based on such a mechanism will ultimately be limited by diffraction and scattering effects when the scales of interest approach the geometrical optics limit.[10]

Using Brewster angle principle is another way to achieve angular selectivity. In 2014, Shen *et al.*[11] achieved angular selectivity of single-polarized light using a quarter-wave stack of isotropic dielectric materials on the basis of Brewster angle theory. Moreover, stacks of photonic crystals were used in metamaterials to produce Brewster angles to achieve broadband angular selectivity.[9] Additionally, a Brewster-like broadband remarkable transmission can be realized at single-polarized incidence[17,18] by using surface plasmons excited by metallic gratings. However, the angular selectivity only be achieved for single-polarized presented in the above-mentioned papers due to theoretical limitations. Subsequently, Shen *et al.*[14] used a uniaxial magnetic dielectric slab theoretically realized dual-polarized angular selectivity based on Brewster angle and critical angles. However, these photonic crystals and anisotropic materials are difficult to fabricate, which can extremely limit its engineering applications.

With the increased use of frequency selective surface (FSS) in microwave engineering, in recent years, the angular selectivity

structure based on FSS is already being explored. Shen *et al.*[15] used double-layer FSS to construct an angle-selective surface (ASS) to achieve angular selectivity in TE-polarization. In addition, the selectivity angle for TE- or TM-polarization can vary from 20° to more than 70° by utilizing an ASS consisting of odd-mode resonant FSS and quarter-wave stacks.[19] Qin *et al.*[20] proposed an efficient synthesis method of ASS based on the accurate equivalent circuit model. Recently, angular selectivity based on a three-layer FSS is proposed,[21] in which the corresponding bandpass condition in terms of the FSS's normalized susceptance is derived. The three-layer FSS structure can then be designed to generate 5% bandwidth of angular sensitivity at TE- and TM-polarization. These approaches proposed a simpler and more robust way than the Brewster angle or critical angles to achieve the angular selectivity. However, most proposed ASS designs based on multiple FSSs are either single-polarized or relatively bulky. There is still a lack of excellent designs to overcome these challenges.

In this Letter, we introduce a simple and yet double-layer FSS structure to achieve angular selectivity for dual polarizations. By properly designing single-layer FSS, polarization-insensitive can be achieved for different incidence angles. Furthermore, the impedance of the double-layer FSS is tuned based on the equivalent circuit analysis to match the free space over a small range of incidence angles. In order to demonstrate the angular selectivity of the dual polarizations, the proposed low-pass ASS is designed and fabricated with an operating frequency of 10 GHz. The design implements the bandpass characteristic ($|S_{21}| > -1$ dB) from 0° to 10° and the band-stop characteristic ($|S_{21}| < -20$ dB) from 31° to 85°. The proposed approach is simple, robust, and scalable, providing a feasible method to achieve a dual-polarized ASS structure.

Figure 1(a) illustrates the concept of our proposed dual-polarized ASS. The properties can be characterized in terms of angular selectivity, with high transmittance at normal incidence and high reflectance at oblique incidence. Although the reflection–transmission characteristics of FSS varies with the angle of incidence,[22] it is difficult for single-layer FSS to produce high transmission at normal incidence.[15] The proposed low-pass ASS structure consists of double-layer FSS with identical top and bottom layers. Through the rational design of constitutive parameters of single-layer FSS, the value of the $\bar{B}_s$ can changes slowly at small angles of incidence and shows a very sharp increase with increasing angle of incidence. Furthermore, based on the equivalent circuit model (ECM), the distance L between the double-layer FSS can be derived, thereby achieving good transmittance at small angles of incidence. As a result, a dual-polarized ASS with high angular selectivity will be achieved. Simulated results show that the proposed low-pass ASS achieves a bandpass ($|S_{21}| > -1$ dB) from 0° to 10° and a band-stop ($|S_{21}| < -20$ dB) from 31° to 85°, with the profile of 0.62 λ.

Figure 1(b) shows the unit cell of single-layer FSS with metallic cross-dipole and metallic grid on the opposite sides of the dielectric substrate, where the top and bottom metallic layers are exactly same and connected by metallic via in the center. The proposed structure is numerically simulated with a commercial time-domain finite element analysis software (CST Studio Suite® 2021). The unit cell boundary condition is applied in x and y directions and open boundary condition is set in the z direction. The Two-Floquet ports with number of two modes are set in the z direction to calculate the transmission coefficient.

Figure 1(c) illustrates the unit cell equivalent circuit model (ECM) of the single-layer FSS that can be modeled as a length of transmission line (TL) paralleled with an open circuit stub. Following the process in papers,[20,23,24] the metallic grids are represented as LC model with a parallel capacitor C_1 and a parallel inductor L_1. The metallic cross-dipole and metallic via are represented as LC model with a parallel capacitor C_2 and two parallel inductors L_2 and L_v, where L_v represents the inductor of the metallic via. βl represents the printed circuit board (PCB) substrates in the TL model, where β is the propagation

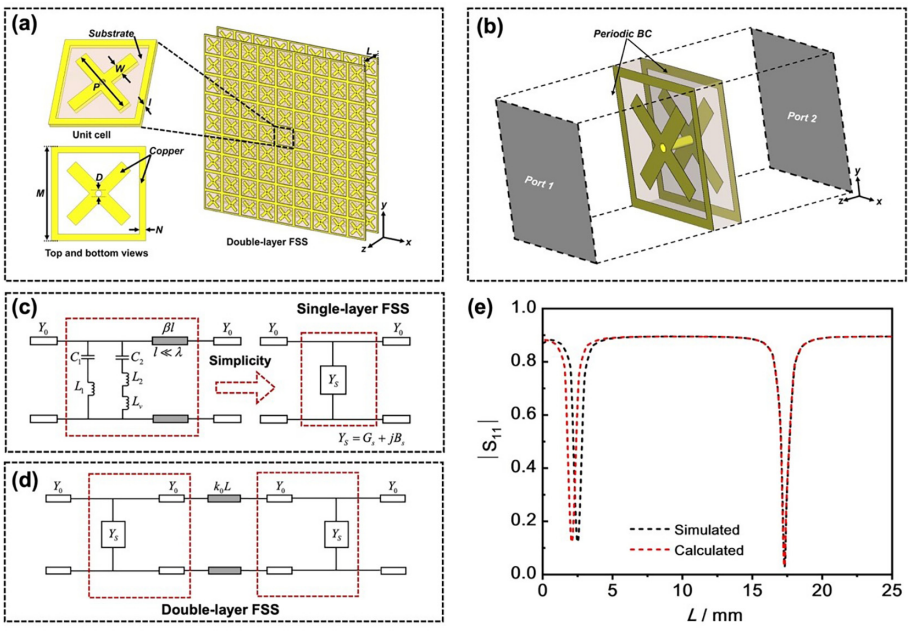

FIG. 1. (a) The design concept for the proposed dual-polarized ASS. (b) The unit cell of single-layer FSS. (c) The equivalent circuit model of single-layer FSS and (d) ASS. (e) The simulated and calculated magnitudes of reflection coefficient $|S_{11}|$ under normal incidence. Geometrical parameters (in millimeters): $p = 12.0$, $W = 2.0$, $l = 0.787$, $D = 0.96$, $M = 14.6$, $N = 1.0$, and $L = 17.3$.

constant. The characteristic admittance of free space is denoted by Y_0. For simplicity, the PCB substrate can be ignored in the ECM analysis because the substrate is very thin ($l \ll \lambda$) and has a low relative permittivity, where λ represents the wavelength corresponding to the operating frequency at 10 GHz.[15]

Then, the equivalent circuit model is simplified as

$$Y_s = G_s + jB_s, \tag{1}$$

where G_s represents conductance, and B_s represents susceptance. Since the structure is lossless, G_s is approximately equal to 0. Because a single-layer FSS of zero thickness and made of perfect electric conductors can be assumed to be lossless, its equivalent circuit model can be easily represented by a shunt susceptance of B_s. The wave admittance of free space is denoted by Y_0 and the normalized susceptance $\bar{B}_s = B_s/Y_0$ is used in the following descriptions. To provide further guidance for this design, the relationship between the normalized susceptance ($\bar{B}_s$) and the reflection coefficient (Γ) is derived as follows:

$$\bar{B}_s = \frac{B_s}{Y_0} = \frac{2\Gamma}{(\Gamma+1)}j. \tag{2}$$

From Eq. (2), it can be seen that there is a proportional relationship between $\bar{B}_s$ and Γ. The value of the $\bar{B}_s$ can be calculated from the $|S_{11}|$ of the designing single-layer FSS. In order to achieve good angular selectivity, the value of the $\bar{B}_s$ of single-layer FSS should be set as follows: changes slowly at small angles of incidence and shows a very sharp increase with increasing angle of incidence. Moreover, in order to achieve dual-polarized stable frequency response at an operating frequency band, electrical length of unit cell is adjusted to eliminate the generation of higher-order mode resonances and grating lobes in a working frequency band.

The ECM of the double-layer FSS is shown in Fig. 1(d). The single-layer FSS are represented as shunt components with a pure imaginary admittance of $Y_s = +jB_s$. Y_0 represents characteristic admittance of the air spacer in the TL model with an electrical length of k_0L, where k_0 is the wavenumber of free space. In order to obtain good transmission performance of the proposed low-pass ASS structure at small angles of incidence, the Γ of double-layer FSS are further derived as

$$\Gamma = \frac{Y_0 - Y_L}{Y_0 + Y_L} = \frac{Y_0 - jB_s - \dfrac{Y_0[Y_0 + (B_s - jY_0)\cot k_0L]}{Y_0 + jB_s - jY_0\cot k_0L}}{Y_0 + jB_s + \dfrac{Y_0[Y_0 + (B_s - jY_0)\cot k_0L]}{Y_0 + jB_s - jY_0\cot k_0L}}. \tag{3}$$

Based on Eq. (3), the bandpass ($\Gamma = 0$) condition is obtained, which is given as

$$\cot k_0L = \frac{B_sB_s}{Y_0(B_s + B_s)} = \frac{B_s}{2Y_0}. \tag{4}$$

The distance L between the two FSS layers can be calculated in accordance with (4) as

$$L = \left[\frac{1}{\pi} \times arc\cot\left(\frac{B_s}{2Y_0}\right) + n\right] \times \frac{\lambda}{2}, \tag{5}$$

where $n = 0, 1, 2 \cdots\cdots$. According to the expression (3) of the double-layer FSS under the normal incidence, the reflection coefficient $|S_{11}|$ magnitude of its equivalent two port network can be calculated. The relationship between $|S_{11}|$ and the distance of the double-layer FSS can be calculated and compared with the simulation results as shown in Fig. 1(e). The numerical analysis and simulation results show good agreement, and the bandpass ($\Gamma = 0$) condition can be expressed as $L = 1.9 + 15 \times n$ (mm), where $n = 0, 1, 2 \cdots$.When $n = 0$, the angular selectivity deteriorates since strong coupling occurs at $L = 1.9$ mm, the optimal value of L is chosen to be the $n = 1$.

Figures 2(a) and 2(b) show the simulated transmission coefficients under TE- and TM-polarization, respectively, for the single-layer FSS at incidence angles ranging from $\theta = 0°$ to 80°. It is observed that the $|S_{21}|$ is −8.7 dB at 10 GHz when $\theta = 0°$ for dual polarizations, showing poor transmittance. As the angle of incidence increases, the $|S_{21}|$ decreases, which are −57.1 and −28.6 dB when $\theta = 80°$ for TE- and TM-polarization, respectively. The simulated $|S_{21}|$ and $\bar{B}_s$ of the single-layer FSS under different angles of incidence for dual polarizations at 10 GHz are shown in Fig. 2(c). For single-layer FSS, the bandstop response under oblique incidence is primarily excited by the electric and magnetic components along the x- and y-directions, rather than the z-direction. This is because the rotated cross and square structures are less sensitive to variations in the z-direction components. However, it is important to note that the z-direction electric and magnetic components play a crucial role in achieving angular selectivity, as they increase with larger incident angles. To better respond to a TM-polarized incident wave under oblique incidence during reflection and transmission, the introduction of via holes along the z-direction can enhance the performance of the sandwich structure FSS. Specifically, the normalized susceptance $\bar{B}_s$ calculated by Eq. (2) is 4.7 at $\theta = 0°$, which is close to 0, and increase with the increasing incident angle. Furthermore, at $\theta = 60°$, the value of $\bar{B}_s$ is significantly different, with 65.9 for TE-polarization and 19.2 for TM-polarization.

In order to realize good transmittance at small angles of incidence, the ASS's structure consisting of double-layer FSS is designed. The distance L between the two FSS layers can be calculated based on Eq. (5). The $L_1 = 1.9$, $L_2 = 16.9$, and $L_3 = 31.9$ mm corresponds to $n = 0$, 1, and 2. When $L = L_3$, the profile of the overall structure is bulky. When $L = L_1$, the angular selectivity deteriorates since strong coupling occurs between the top and bottom layers. In addition, the optimal value of L_2 may be slightly different from the calculated value due to the presence of the PCB substrate. Finally, the optimal distance of $L_2 = 17.3$ mm is chosen in our design through the full-wave simulation method. The simulated transmission coefficients of the ASS under the dual-polarized incidences of $\theta = 0°$ to 80° are shown in Figs. 2(d) and 2(e). It is observed that the $|S_{21}|$ is −0.2 dB at 10 GHz when $\theta = 0°$ for dual polarizations. As the angle of incidence increases, the $|S_{21}|$ decreases, which are −46.5 dB for TE-polarization and −37.6 dB for TM-polarization when $\theta = 80°$. Moreover, Fig. 2(f) shows the transmission coefficients of the ASS under the dual polarizations with various incident angles at 10 GHz. When the incident angle is less than 10°, $|S_{21}|$ is greater than −1 dB and decreases as the incident angle increases. As the angle of incidence increases to 30°, $|S_{21}|$ drops to −20 dB, proving that good angular selectivity is realized.

In order to validate the design concept and evaluate the performance of the angular selectivity, the designed ASS is fabricated and measured. Figure 3(d) shows fabrication prototype of the ASS. The samples are fabricated by a standard printing circuit board technology. The copper patterns (thickness, 0.018 mm) are periodically printed on

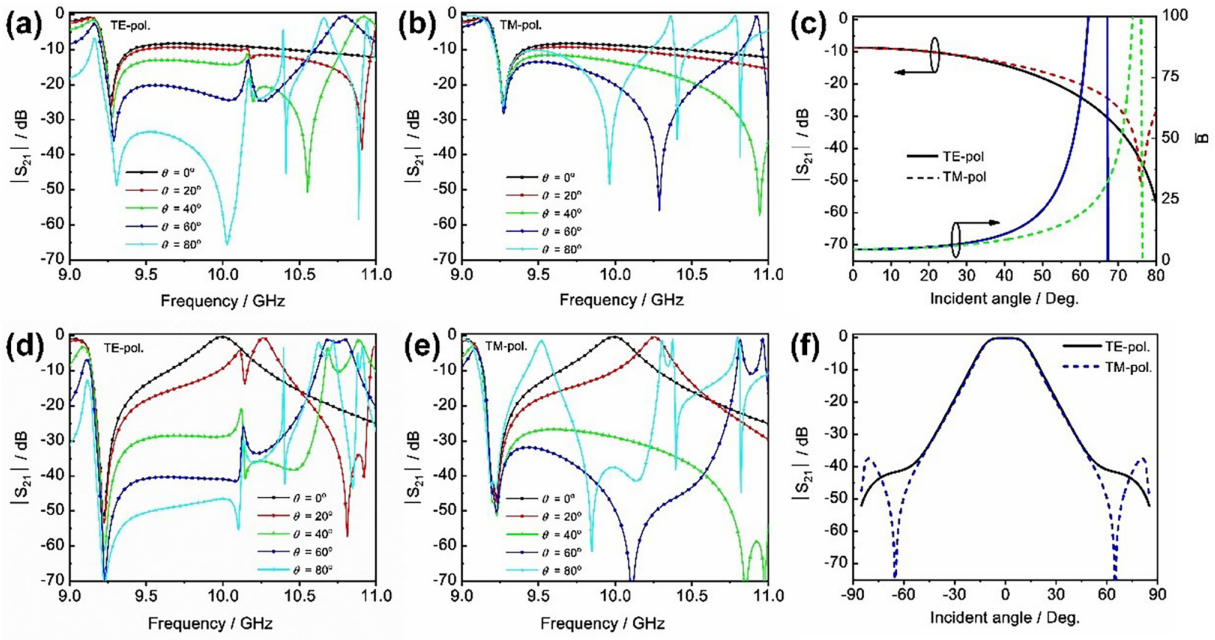

FIG. 2. Simulated transmission coefficients ($|S_{21}|$) of the proposed ASS structure under different polarizations and incident angle. Single-layer FSS with (a) TE-polarization, (b) TM-polarization, and (c) dual polarizations for different incident angles at 10 GHz. ASS structure with (d) TE-polarization, (e) TM-polarization, and (f) dual polarizations for different incident angles at 10 GHz.

both sides of the RT/Duroid 5880 high frequency substrate (thickness, 0.787 mm, tangential loss, 0.001 at 10 GHz) with a permittivity of 2.2. Next, the two FSS layers are mounted through plastic screws. The sample consists of 21 × 21 unit cells, the totally size of the sample is 306.6 × 306.6 mm^2 (10 λ at 10 GHz).

Figure 3(c) shows the measurement setup. The measurement of $|S_{21}|$ is carried out in an anechoic chamber. Two standard linearly polarized horn antennas connected to a vector network analyzer (VNA, Agilent E8362B) serve as transmitter and receiver to measure the transmission magnitude of the sample. The distance between antennas and the sample is set far enough to avoid near-field effect. As shown in Figs. 3(a) and 3(b), the open aperture and metal plane on the sample holder were calibrated prior to the measurement, and the sample holder rotates from 0° to 80° with a sampling interval of 10°. To

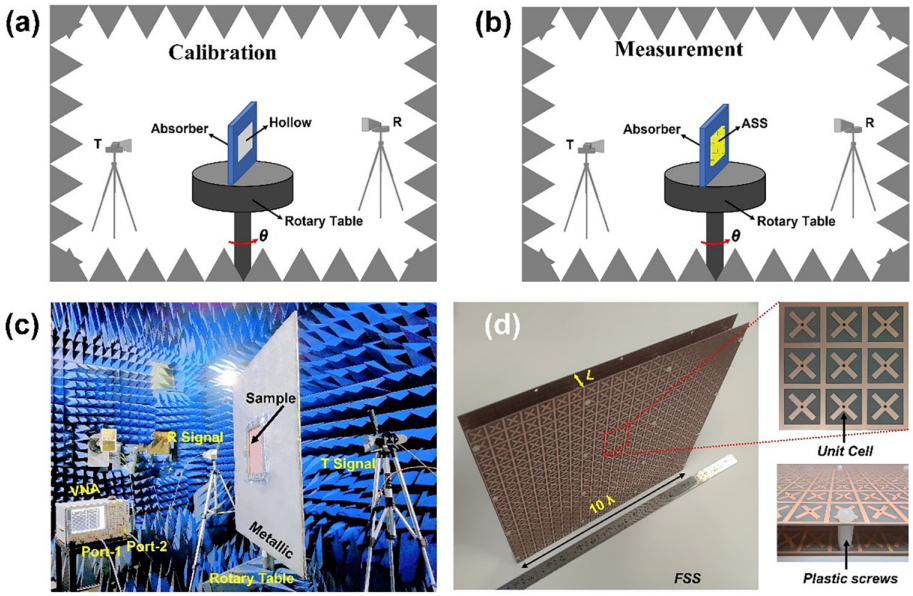

FIG. 3. Transmission coefficients measurement setup for ASS: (a) calibration, (b) measurement, and (c) measurement equipment. (d) Fabrication prototype of the ASS.

eliminate multi-path transmission signals in the measurements, time-domain gating was used in the VNA analysis. Finally, the transmission coefficients of the sample can be achieved by

$$|S_{21}|_{\text{sample}} = \frac{|T_{21}|_{\text{sample}}}{|T_{21}|_{\text{air}}}, \tag{6}$$

where $|T_{21}|_{\text{air}}$ and $|T_{21}|_{\text{sample}}$ are the measured transmission magnitude without and with the ASS sample, respectively.

Figures 4(a)–4(d) show the simulation and measured transmission coefficients of the proposed low-pass ASS for dual polarizations from $\theta = 0°$ to 80° at different frequencies. The measured and simulated transmittance results at 10 GHz under dual polarizations are compared in Fig. 4(e), where the simulated results are in good agreement with the measured ones at different incident angles. At larger angles of incidence, there is a small deviation between the measured and simulated results, which may be caused by factors, such as the low radiated power of the transmitter antenna. Figure 4(f) shows the simulated electric field distributions of the proposed low-pass ASS structure at 10.0 GHz, where good selectivity of the electric field distributions is realized as the angle of incidence increases.

The proposed low-pass ASS is compared with previously published angular selectivity structures in the literature in terms of polarization and other performance characteristics and presented in Table I. In this table, it can be found that the structures in Refs. 11 and 9 only achieves single-polarized angular selectivity based on photonic crystals. Although the structure in Ref. 14 achieves angular selectivity under dual polarizations, the structure based on uniaxial dielectric–magnetic material is difficult to fabricate. It is worth mentioning that the structures in literatures (Refs. 15 and 19) are based on the FSS, which is simple and easy to fabricate; however, the structures only achieve single-polarized angular selectivity. Furthermore, the three-layer FSS structure in Ref. 21 achieve dual-polarized angular selectivity. It is evident from Table I that the proposed ASS is not only dual-polarized but also has the thinnest thickness with a simple structure based on double-layer FSS. Moreover, the proposed low-pass ASS achieves good angular selectivity with a passband ($|S_{21}| > -1$ dB) from 0° to 10° and a stop band ($|S_{21}| < -15$ dB) from 26° to 85°.

In summary, a double-layer ASS structure based on double-layer FSSs has been studied for providing angular selectivity under dual polarizations. An equivalent circuit model is used to analyze the structure. The properly designed FSS has a normalized susceptance $\bar{B}_s$ close to zero under the normal incidence; however, when the angle of incidence increases, the value of $\bar{B}_s$ increases sharply. Then, the low-pass ASS structure was designed based on the equivalent circuit analysis, which achieves good angular selectivity with a passband ($|S_{21}| > -1$ dB) from 0° to 10° and a stop band ($|S_{21}| < -15$ dB) from 26° to 85°. The proposed low-pass ASS is fabricated and measured at an operating frequency of 10 GHz, where the simulated results are in good agreement with the measured ones at different incident angles. Good angular selectivity has been demonstrated. The proposed low-pass ASS structure that is planned to be used as a feeder for solar radio telescopes to achieve high spatial resolution characteristics by reducing the side lobes of the array antennas. In addition, in order to obtain a wide bandwidth angular transmission response, in the future work, we would like to introduce dielectric ceramic substrates with high dielectric constants or use three-dimensional structures of FSS to realize low-profile and wide-bandwidth angular selective surfaces.

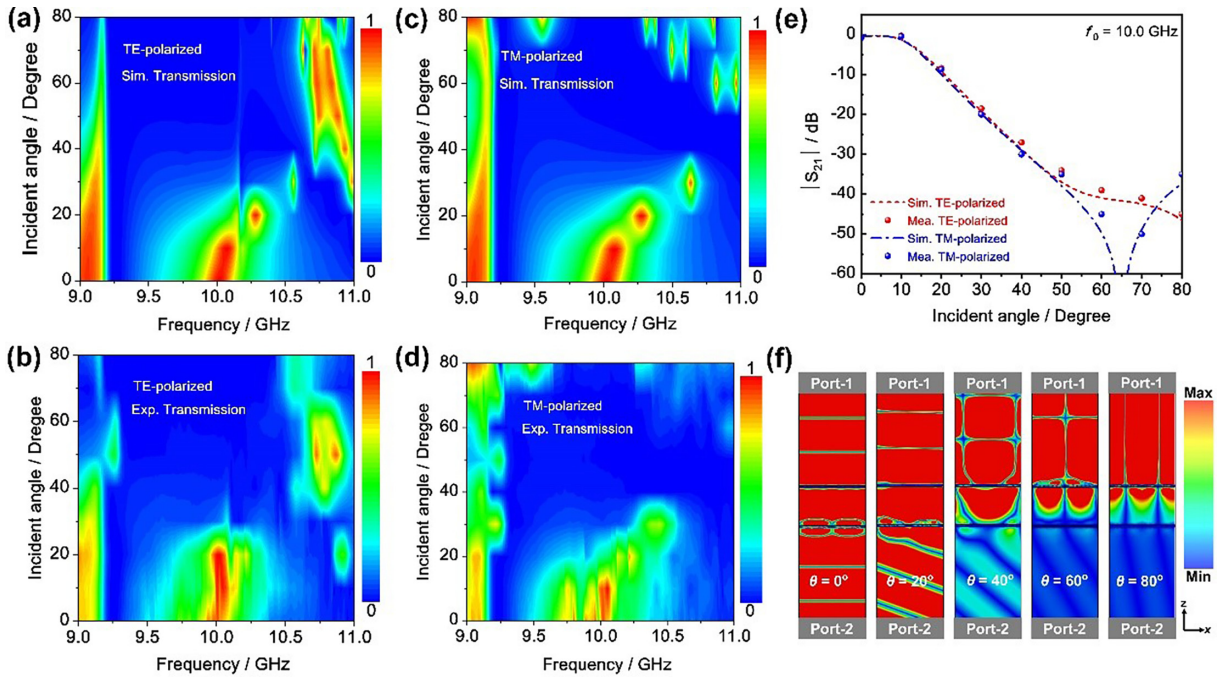

FIG. 4. Transmission magnitudes ($|S_{21}|$) of the proposed ASS structure under different incident angle. Simulation results under (a) TE-polarization and (b) TM-polarization. Experimental measurement results under (c) TE polarization and (d) TM-polarization. (e) Simulation and experimental measurement results for dual polarizations under different angles of incidence at 10.0 GHz. (f) Simulated electric field distributions of the proposed low-pass ASS structure under different incidence angles at 10.0 GHz.

TABLE I. Comparison of the performance with previously published angular selectivity structures.

References	Polarization	Structure	Thick (λ)	Angular selectivity	
				Bandpass ($\|S_{21}\| > -1$ dB)	Band-stop ($\|S_{21}\| < -15$ dB)
11	Single	Photonic crystals	$\gg$1.0	Brewster angle	Every other angle
9	Single	Anisotropic dielectric	$\gg$1.0	From 0° to 20°	Every other angle
14	Dual	Uniaxial dielectric	1.0	Brewster angle	Critical angle
15	Single	FSS	0.7	From 0° to 16°	From 40° to 80°
19	Single	FSS	3.1	30°	Every other angle
21	Dual	FSS	1.1	From 0° to 15°	From 30° to 60°
This work	Dual	FSS	0.6	From 0° to 10°	From 26° to 85°

This work was supported by the National Natural Science Foundation of China (Nos. 52202114 and 52202146), the International Cooperation Project of Shaanxi Province (No. 2021KWZ-10), the Shaanxi Provincial Department of Education (No. 22JK0275), the Zhejiang Provincial Science and Technology Program (No. LGG20F010007), the Fundamental Research Funds for the Central University, and the 111 Project of China (No. B14040). The authors gratefully acknowledge the financial support from China Scholarship Council (Grant No. 202106280265).

AUTHOR DECLARATIONS

Conflict of Interest

The authors have no conflicts to disclose.

Author Contributions

Chao Du: Conceptualization (lead); Data curation (lead); Investigation (lead); Project administration (lead); Software (lead); Writing – original draft (lead). **Huizhen Chen:** Formal analysis (equal); Resources (equal); Software (equal); Supervision (equal); Writing – original draft (equal). **Shaofei Wang:** Data curation (equal); Methodology (equal); Software (equal). **Yongqiang Pang:** Resources (equal); Visualization (equal); Writing – review & editing (equal). **Tao Zhou:** Investigation (equal); Project administration (equal); Resources (equal). **Song Xia:** Resources (equal); Supervision (equal); Validation (equal). **Di Zhou:** Conceptualization (equal); Funding acquisition (lead); Project administration (lead); Writing – review & editing (lead).

DATA AVAILABILITY

The data that support the findings of this study are available from the corresponding author upon reasonable request.

REFERENCES

[1]A. Alu, G. D'Aguanno, N. Mattiucci, and M. J. Bloemer, Phys. Rev. Lett. **106**, 123902 (2011).
[2]N. Aközbek, N. Mattiucci, D. de Ceglia, R. Trimm, A. Alù, G. D'Aguanno, M. A. Vincenti, M. Scalora, and M. J. Bloemer, Phys. Rev. B **85**(20), 205430 (2012).
[3]E. D. Kosten, J. H. Atwater, J. Parsons, A. Polman, and H. A. Atwater, Light. Sci. Appl. **2**(1), e45 (2013).
[4]Y. P. Shang, Z. X. Shen, and S. Q. Xiao, IEEE Trans. Antennas Propag. **61**(12), 6022 (2013).
[5]Z. B. Zhu, Y. F. Li, J. Q. Zhang, J. F. Wang, W. P. Wan, L. Zheng, M. D. Feng, H. Y. Chen, and S. B. Qu, Opt. Express **29**(3), 4219 (2021).
[6]H. F. Ma, G. Z. Wang, G. S. Kong, and T. J. Cui, Opt. Mater. Express **4**(8), 1717 (2014).
[7]F. Zeng, L. F. Ye, L. Li, Z. H. Wang, W. Zhao, and Y. Zhang, Opt. Express **27**(23), 33826 (2019).
[8]T. J. Cui, M. Q. Qi, X. Wan, J. Zhao, and Q. Cheng, Light. Sci. Appl. **3**(10), e218 (2014).
[9]Y. C. Shen, D. X. Ye, L. Wang, I. Celanovic, L. X. Ran, J. D. Joannopoulos, and M. Soljačić, Phys. Rev. B **90**(12), 125422 (2014).
[10]Y. C. Shen, C. W. Hsu, Y. X. Yeng, J. D. Joannopoulos, and M. Soljačić, Appl. Phys. Rev. **3**(1), 011103 (2016).
[11]Y. C. Shen, D. X. Ye, I. Celanovic, S. G. Johnson, J. D. Joannopoulos, and M. Soljačić, Science **343**(6178), 1499 (2014).
[12]P. R. Franchi and R. J. Mailloux, IEEE Trans. Antennas Propag. **31**(3), 445 (1983).
[13]Y. Lee, S. H. Jeong, W. S. Park, J. S. Yun, and S. I. Jeon, in *IEEE MTT-S International Microwave Symposium Digest* (IEEE, Seattle, WA, USA, 2002), pp. 1329–1332.
[14]H. Huang and Z. X. Shen, Antennas Wireless Propag. Lett. **19**(12), 2457 (2020).
[15]L. Zhou and Z. X. Shen, Opt. Express **29**(13), 20379 (2021).
[16]J. H. Atwater, P. Spinelli, E. Kosten, J. Parsons, C. V. Lare, J. V. de Groep, J. G. de Abajo, A. Polman, and H. A. Atwater, Appl. Phys. Lett. **99**(15), 151113 (2011).
[17]C. Argyropoulos, G. D'Aguanno, N. Mattiucci, N. Akozbek, M. J. Bloemer, and A. Alù, Phys. Rev. B **85**(2), 024304 (2012).
[18]Y. Xie, A. R. Zakharian, J. V. Moloney, and M. Mansuripur, Opt. Express **14**(22), 10220 (2006).
[19]N. Kou and S. X. Yu, Antennas Wireless Propag. Lett. **21**(11), 2151 (2022).
[20]T. Qin, X. Q. Lin, Y. Yao, Y. Liu, H. Liu, P. Hao, and P. Mei, IEEE Trans. Microwave Theory Tech. **71**(6), 2625 (2023).
[21]Z. Chen, C. Du, J. Liu, D. Zhou, and Z. Shen, IEEE Trans. Antennas Propag. **71**(11), 8704 (2023).
[22]B. A. Munk, *Frequency selective surfaces: theory and design* (John Wiley & Sons, 2000).
[23]F. Costa, A. Monorchio, and G. Manara, IEEE Antennas Propag. Mag. **54**(4), 35 (2012).
[24]F. Costa, A. Monorchio, and G. Manara, Appl. Comput. Electromagn. Soc. J. **29**(12), 960–973 (2014).